NASA
Technical
Paper
2851

November 1988

Lightweight Structural Design of a Bolted Case Joint for the Space Shuttle Solid Rocket Motor

John T. Dorsey,
Peter A. Stein,
and Harold G. Bush

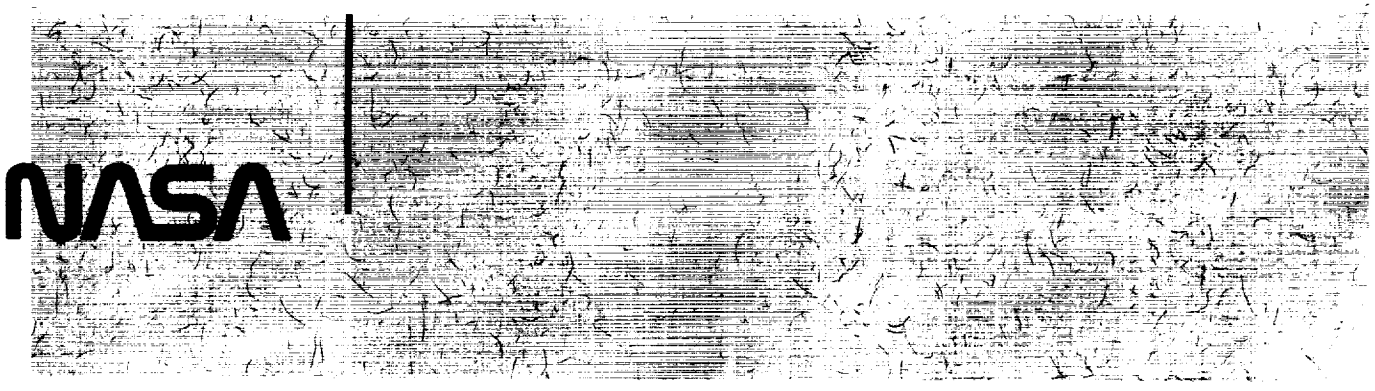

NASA Technical Paper 2851

1988

Lightweight Structural Design of a Bolted Case Joint for the Space Shuttle Solid Rocket Motor

John T. Dorsey
Langley Research Center
Hampton, Virginia

Peter A. Stein
U.S. Coast Guard Station
Yorktown, Virginia

Harold G. Bush
Langley Research Center
Hampton, Virginia

National Aeronautics and Space Administration

Scientific and Technical Information Division

Introduction

The Space Shuttle solid rocket motor (SRM) consists of 11 separate weld-free steel segments (cylindrical shells) approximately 12 ft in diameter. Adjoining case segments are mechanically assembled using tang-clevis joints, with each joint having 180 steel pins around its circumference (fig. 1). An investigation by an independent Presidential committee determined that the loss of the Space Shuttle Challenger (flight 51-L) was most likely due to failure of the O-ring seals in the aft field joint (ref. 1). After the accident, NASA initiated the Advanced Solid Rocket Motor Program with the objective of devising new and innovative ways to join solid rocket motor case segments, which might be used to upgrade the current system.

This paper describes a bolted joint concept that provides an alternate method for joining SRM case segments. This concept uses a static face seal between two opposing flanges to prevent hot gas leakage and redirects internal forces around the bolts to reduce gap opening moments. A design requirement for the bolted joint concept is that no gap exist between the two flanges at the O-ring location during firing of the SRM. One objective of this study is to characterize parametrically the structural behavior of a bolted joint and to quantify the influence of the various design parameters on joint structural performance and mass. A second objective is to examine ways of reducing high stresses identified in references 2, 3, 4, and 5. A third objective is to determine a set of design parameters which (1) meets the design requirement of keeping the joint closed at the O-ring locations at all times and (2) limits the joint mass to a minimum practical value.

Bolted Joint Concept

The proposed concept, shown in figure 2, is similar in appearance to the bolted flange joints used in industry to connect pipes. The joint uses studs and nuts to hold two opposing flanges together and to seat (that is, compress) the two polymeric O-rings. The studs are recessed into alcoves that are machined (or forged) into the shell wall, and bearing plates are used to transfer the compressive loads from the nuts into the flanges. A shear lip helps align case segments during assembly. Gussets between the alcoves provide a path to transfer the axial load from the shell wall into the flanges between the bolts. The materials and associated properties for the various joint components are summarized in table I.

Industry practice for pressure vessel design is to use very thick flanges that have sufficient bending stiffness to prevent any deflection (or gaps) from occurring at the O-ring locations under applied internal pressure loading. The resulting designs are, in general, too heavy for aerospace applications. Rather than depend on flange thickness to prevent deflections at the O-rings, the present concept redirects pressure-induced internal forces in the shell wall to keep the SRM joint closed and the O-rings sealed, as shown in figure 3. Because of its high hoop stiffness, the flange undergoes less radial displacement than does the shell wall away from the joint. This differential displacement creates a moment on the flange which tends to lift the inner part of the joint and enlarge the gap at the O-rings.

Figure 3 illustrates the results of offsetting the stud centerline with respect to the center of the shell (motor case) wall. This offset, referred to as eccentricity, is positive when the stud centerline is radially outside the shell wall centerline. The dashed lines represent deflection of the flange faces caused by the booster internal pressure loading components. The radial pressure component on the shell wall always acts to open the flange faces at the inside of the joint (where the O-rings are located) no matter what value of eccentricity is chosen. Negative eccentricity, however, can be used to transfer the pressure-induced axial load from the shell wall into the gussets between the bolts, thus reducing the opening moment. When sufficient negative eccentricity is chosen, the moment about the stud closes the joint at the O-rings.

The structural behavior and mass of the bolted joint concept are directly related to values chosen for the major design variables. The particular variables studied herein are (1) the number and size of the studs used, (2) eccentricity, (3) use of a bearing plate, (4) gusset thickness, and (5) flange thickness.

The stud diameter has a major impact on joint mass because minimum flange width is dictated by the size of the associated nut. Widening the flange adds mass and increases the structural hoop stiffness at the joint, resulting in larger joint opening at the O-rings. Thus, it is desirable to use the smallest practical stud size in the design. If stud size is too small, however, the number of studs required to carry the load increases to the point where the gusset thickness is too small for adequate load transfer. On the other hand, if too few studs are used, the axial load can cause gaps to open under the gussets because of excessive stud spacing. To minimize joint opening, the number of studs required must be determined in concert with the gusset area required to keep gusset stresses at an acceptable level. The maximum pretension load for each stud was 70 percent of the stud ultimate strength, which is consistent with the specified design factor of safety of 1.4.

Gusset thickness depends not only on the number of studs used, but also on whether a bearing plate is used. Figure 4 shows the relationship between gusset thickness and nut size for both the unmodified flange and the bearing-plate concepts and illustrates one advantage of using a bearing plate. The bearing plate acts as a form-fitted washer, allowing a smaller clearance between the nut and the gusset (see fig. 4 insets). Thus, for a given number of studs, a bolted joint incorporating a bearing plate can have thicker gussets (resulting in reduced gusset axial stress) than an unmodified design. A second advantage of a bearing plate is that, for a given total flange thickness, a bearing-plate/flange combination has less hoop stiffness than a solid flange. Reduced hoop stiffness is beneficial because it helps close the joint in the vicinity of the O-rings.

Finite-Element Model Description

The finite-element analysis is used to determine the behavior of the bolted joint as some of the major design parameters are varied, to arrive at the combination of design parameters that gives the best performance for the minimum structural mass.

Because the joint geometry repeats at each stud location around the circumference of the booster, only a representative sector of the joint and shell wall (from the centerline of a stud to the center of an adjacent gusset) had to be modeled. In addition, a plane of symmetry was assumed at the interface between two case segments so that only the top (or bottom) half of a joint had to be analyzed. Finally, analytical results given in reference 6 for the SRM show that the stress field is essentially uniform beyond 18 in. from any location where the shell stiffness changes (at a joint, for example). Thus, the joint model included only the first 22 in. in length from the case segment interface.

To simulate the contact problem between two joint halves and to predict the general three-dimensional stress state throughout the joint and shell, three-dimensional elastic finite elements were used in the analysis. The structural analysis code Engineering Analysis Language (EAL), used for all analyses, has three-dimensional elements that are based on the assumed-stress hybrid formulation (ref. 7). The contact problem between two joint faces was modeled using a gap-contact element described in reference 8 and required nonlinear analysis capability.

Two levels of finite-element models were used in the study. For the large number of parametric studies performed in the beginning, a joint model with a coarse mesh was used to study a large number of effects without incurring a large computational expense. After major design parameters were fixed, a refined mesh model of the joint was developed. The refined model included details such as the two O-ring grooves and the shear lip and could be used to represent both joint halves: the O-ring side including the shear lip, and the opposing flat side without grooves.

Model Assembly

The coarse finite-element model, shown in figure 5, consisted of either two or three separate components: the flange/gusset/shell, the stud/nut, and the bearing plate. Complete structural models of the joint were made by assembling the required components with gap-contact elements (having infinite stiffness in compression and zero stiffness in tension) and zero-length rigid elements. When a bearing plate was included in the model, the contact elements were used to connect nodes on the bottom of the bearing plate to coincident nodes on the top of the flange.

The stud/nut component was attached either to the top of the flange or, when a bearing plate was present, to the top of the bearing plate. In either case, the bottom of the nut remained in contact with the top of the flange or bearing plate under all loading conditions, and thus zero-length rigid elements were used in this region of the model. Contact elements were used, however, between the stud and the sides of the stud hole in the flange to model any contact that might occur. The contact elements in this region allow 0.005 in. of relative closure (equal to the tolerance between the stud and the hole) between adjacent nodes on the stud and flange before becoming rigid. Contact between the stud and flange would require severe flange bending, something that never occurred in the present study.

Boundary Conditions

Assuming circumferential periodicity allowed reduction of the joint model to an approximately 1° (180° divided by the number of studs) sector of the motor case. The boundary conditions required constraining the circumferential degree of freedom at each node on the two constant-theta planes as shown in figure 6, but allowed radial (R) and longitudinal (Z) displacements. Because the joint was a wedge, any movement in the radial direction would result in circumferential boundary forces on the two constant-theta planes and, thus, no radial constraints were required for the model. Assuming symmetry at the interface of two SRM segments required that all nodes at the bottom of the stud be constrained in the Z-direction. For the flange bottom, no constraints were required in the Z-direction because the contact elements assured that these nodes would not penetrate the Z-symmetry plane.

Applied Loading

The clamping force imparted by the stud/nut combination to the opposing flanges in the joint was simulated in the finite-element model by a thermal prestress in the stud. A negative temperature increment was applied to the elements making up the stud, causing the stud to contract in the Z-direction. Because the nut and stud were modeled as one component, this contraction caused the nut to compress the flange (and bearing plate, when present) and preload the joint. The temperature was adjusted so that the sum of the reactions at the bottom of the stud was 70 percent of the stud ultimate load.

After the stud was preloaded, loads corresponding to the internal booster pressure were applied. A radial pressure load of 1000 psi was applied to the inside wall of the booster, as shown in figure 6. The total axial load, the product of the internal pressure and the area of the forward dome, is approximately 16.5 million lbf, or 36 300 lbf per inch of booster circumference. The axial load was distributed uniformly along the top of the shell wall, as shown in figure 6. These loading conditions were developed in reference 8 as a worst case, with the 1000 psi pressure being slightly higher (approximately 2 percent) than the maximum design pressure.

Because the O-ring grooves were included in the refined model, an important modification to the pressure load distribution was required. The assumption was made that, even if no gap existed at the inside of the joint, pressure could pass to the inside O-ring (and no farther, as long as the O-ring maintained a seal). Thus, the pressure loading was assumed to be distributed along the bottom and inside surfaces of the shear lip and along the bottom of the flange to the inner O-ring groove, as shown in figure 7(a). On the flat side of the joint, pressure loading was included on the bottom of the joint to the point where the opposing O-ring made contact (see fig. 7(b)).

The polymeric O-rings are compressed when joint halves are mated during assembly, resulting in a load of approximately 25 lb/in. per seal acting to open the joint (see ref. 3). Since the O-ring load is very small relative to all other applied loads, it was not included in the analysis.

Joint Structural Performance

As stated in the introduction, one objective was to design a joint that stays closed throughout pressurization of the SRM. In particular, the area between the O-rings and the inside of the booster must stay closed under the applied loadings. Consequently, in the initial parametric studies, emphasis was placed on determining the range of design variables that maintained closure of the inner part of the joint. Any locations of high stress were addressed after values for the major design variables were chosen.

Displacements and Gaps

Key locations on the flange bottom of the coarse and refined models are shown in figures 8(a) and 8(b), respectively. (The effects of splitting the flange and cutting slots in the flange will be discussed in subsequent paragraphs.) In the coarse model, locations C1 through C3 were on the inside edge of the flange, and locations C4 and C5 were on a line approximately halfway between the two O-rings. In the refined model, locations R1 and R2 were on the inside edge of the shear lip, while R3 and R4, and R5 and R6 were on the inside edges of the inner and outer O-ring grooves, respectively. Gap locations were identical for the O-ring and flat halves of the joint. In the analysis, the displacements given by the gap-contact elements on the flange bottom were the distance between the flange and the symmetry plane, that is, half the total gap between two opposing flanges. The total gap value is given throughout this report.

Coarse model. In figure 9, gaps at three locations on the flange bottom are shown as stud eccentricity is varied for the coarse model with the following properties: 170 $1\frac{1}{16}$-in-diameter studs, 1-in-thick flange, and stud preload of 70 percent of ultimate load (F_{ult}). The gaps on the inside of the joint (C1 and C3) decrease dramatically as the stud centerline moves radially inward, with the gap under the gusset center (C3) decreasing from 9.07 mils for zero eccentricity, to 0.34 mil at an eccentricity of −0.5 in. At the approximate O-ring location (C5), the gap is only 0.12 mil for an eccentricity of −0.5 in. For a basis of comparison and a practical limit on defining a zero gap, the typical surface texture design requirement for machined mating surfaces (static) is 0.125 mil (see ref. 9). The change in joint mass associated with moving the stud was found to be 8.0 lbm per 0.1 in. of eccentricity. The sensitivity of gap opening, taken with the associated small mass penalty, indicates that stud eccentricity is an efficient parameter for designing bolted joints that remain closed under internal pressure loading.

The contact region of the flange bottom is shown for eccentricities of 0 and −0.5 in. in figures 10(a) and 10(b), respectively. As the stud centerline was moved radially inward, the contact region between two opposing flanges moved from the outer to the inner part of the joint. The gap (0.34 mil) at location C3 in figure 10(b) is due to the Poisson effect caused by initially prestressing the stud and compressing the flange. This Poisson effect is illustrated

in table II, where the gap at locations C2, C3, and C5 is shown to decrease when the stud preload is decreased while the SRM is pressurized to 1000 psi.

A simple way to reduce the flange hoop stiffness is to cut, or split, the flange outboard of the stud along the radial plane through the stud centerline, as shown in figure 8(a). In the finite-element model, this effect was achieved by removing the circumferential constraints on the nodes in the indicated location. Figure 11, which shows the radial displacement of the nodes on the inside wall (as indicated by the heavy line) of the model from the flange bottom to the top of the shell, illustrates that splitting the flange allows the flange radial displacement to approximate more closely the shell far-field displacement.

Figure 9 illustrates the effect of splitting the flange. The gap at location C3 was reduced to less than 0.5 mil at an eccentricity of −0.2 in. It is shown in figure 9 that a gap this small was not achieved with a solid flange until stud eccentricity reached a value of −0.5 in. However, splitting the flange reduces the bending stiffness as well as the hoop stiffness, resulting in larger gaps on the outer part of the joint (6.56 mils versus 4.56 mils for location C7 at an eccentricity of −0.5 in., for example). Since gaps outside the seal locations of the joint are not critical, small displacements along the outside edge appear acceptable.

For a given total thickness, a flange/bearing-plate combination has less bending and hoop stiffness than a solid flange, with the stiffness reductions being a function of the ratio of bearing-plate thickness to total thickness. In table II, gaps for a joint with a solid 1-in-thick flange are shown in comparison with gaps for joints with flange thicknesses of 3/4 in., 1 in., and 1¼ in., all with a 1/4-in-thick bearing plate. All 4 joint configurations have 170 1 1/16-in-diameter studs, eccentricity of −0.5 in., and a stud preload of $0.7F_{ult}$.

For the flange/bearing-plate combination model, gaps on the inner part of the joint (locations C2–C5) are smaller than corresponding gaps for the solid flange of the same thickness (1 in. total) because of the reduced hoop stiffness of the joint. Conversely, gaps on the outer part of the joint (location C7) are larger because of reduced bending stiffness. The results in table II are consistent with the radial displacements shown in figure 11, in that the flange/bearing-plate model results fall between the solid flange and the split flange data.

When a flange/bearing-plate combination with a thickness ratio of 1 in./0.25 in. and a solid flange (1 in. thick) were considered, gaps on the inner part of the joint were approximately 30 percent larger in the flange/bearing-plate model than in the solid flange model. This occurred because the gusset in the flange/bearing-plate model was 0.633 in. wide, compared with only 0.483 in. in the solid flange model. The increased gusset width in the flange/bearing-plate model provided greater hoop stiffness, which led to larger gaps on the inner part of the joint. Also, increasing the flange thickness (up to 1¼ in.) did not reduce the gaps on the inner part of the joint.

In table III, gaps at the inner part of the joint are shown for models with 180 1-in-, 170 1 1/16-in-, and 166 1 1/16-in-diameter studs. The results in table III are for a model with a solid 1-in-thick flange (no bearing plate), eccentricity of −0.5 in., and a stud preload of $0.7F_{ult}$. The results show that increasing the number of studs reduced the gaps at the inner part of the joint. In this design study, 1-in-diameter studs were found to be the smallest practical size when the trade-off between total stud area and total gusset area was considered. To provide a point of comparison, however, the design with 170 1 1/16-in-diameter studs was analyzed in subsequent studies.

Refined model. The added detail of the refined model enabled the gaps at the edge of the O-ring grooves to be determined. Gaps on the O-ring side of the joint are shown in comparison in table IV for designs with 170 1 1/16-in-diameter studs and 180 1-in-diameter studs, for a flange/bearing-plate thickness ratio of 0.75-in/0.25-in., an eccentricity of −0.5 in., and a stud preload of $0.7F_{ult}$. In general, gaps on the inner part of the joint were smaller for the design with 180 1-in. studs than for 170 1 1/16-in. studs, although both designs showed complete closure at the inside edge of the inside O-ring groove.

In table V, gaps are shown for various cases of a joint design that had 180 1-in-diameter studs, a flange/bearing-plate thickness ratio of 0.75-in/0.25-in., and a stud preload of $0.7F_{ult}$. (All table entries referring to slots and alcove modifications are discussed in the section on stresses.) The first two entries establish the baseline performance of the design with 180 1-in. studs and show the behavior of opposing joint halves to be nearly identical. The results also quantify those design parameters that prevent gaps at the O-ring location during SRM pressurization.

Stresses

Allowable stresses in the model, defined by dividing the material tensile ultimate strength by a factor of 1.4, are listed in table I. The 2:1 biaxial stress field in the far-field motor case permits a 7.1-percent increase in allowable stress, giving a value of 153 ksi for the motor case (unpublished results from Wasatch Division, Morton Thiokol Inc., 1981). Except where otherwise noted, all stresses quoted in this report are

element bulk stresses, which are calculated by averaging the element nodal stresses (8 corners of a brick, 6 corners of a wedge, and 4 corners of a pyramid).

Locations in the shell, gusset, or flange where stresses exceed 143 ksi are shown in figure 12 for the coarse model with 170 $1^{1}/_{16}$-in-diameter studs, an eccentricity of −0.5 in., a flange thickness of 3/4 in., and a bearing-plate thickness of 1/4 in. Calculated values of far-field circumferential stress, 157 ksi, and axial stress, 77 ksi, are identical to those obtained with the refined model and compare well with values from reference 8 (155 ksi and 76 ksi, respectively). The far-field stress exceeds the allowable stress by the same percentage that the 1000 psi pressure load exceeds the SRM design pressure.

High local stress occurred where a wedge-shaped transition section from the shell wall to the gusset intersected the gusset (location A in fig. 12). Because localized fillet details were not included in the model, a sharp corner existed there. The highest stress at this location was $\sigma_Z = 149$ ksi in the unmodified coarse model (155 ksi in the unmodified refined model as shown in fig. 13). When a slight fillet was introduced into the model, the maximum stress in this region dropped to an acceptable value of 134 ksi. (The fillet was not added to the refined model; however, lower stresses, on the order of 10 percent, are expected if the fillet is added.)

Another location of high stress existed at the top of the alcove where the transition wedge intersected the shell wall (location B in fig. 12). Once again, since no material tailoring or filleting had been done in this region of the model, a sharp corner existed (also see fig. 14(a)), which resulted in $\sigma_\theta = 185$ ksi in the element shown. Tailoring the alcove (by removing material) in the refined model to the geometries shown in figures 14(b) and 14(c) reduced this stress to 155 ksi for the intermediate-alcove geometry and to 149 ksi for the wide-alcove geometry. Reference to table V shows that the alcove modifications caused very small gap openings at the O-ring grooves—less than 0.3 mil for the intermediate alcove and less than 0.4 mil for the wide alcove. However, the alcove modifications increased the axial stress in the gusset by 8 percent for the intermediate alcove and 14 percent for the wide alcove. These stress increases would probably be mitigated by gusset tailoring, which was not done in these models.

The stress concentration at location C is a consequence of the joint geometry and loading. The flange (having a very large radius of curvature) acts essentially like a finite-width plate, with a hole, subjected to a uniaxial tensile load (caused by the circumferential stress induced by the internal booster pressure) and thus closely adheres to the classical solution for stress concentration at the edge of a hole. The largest elastic stress, $\sigma_\theta = 278$ ksi, occurred on the outside bottom edge of the hole (location C_{outer} in fig. 12) in the 3/4-in-thick flange design. Although the stresses quoted at the edge of the hole are significantly above yield, they are useful because they indicate the stress concentration severity. For comparison, analysis of the original tang-clevis joint showed a peak elastic stress of 249 ksi at the edge of the shear pin holes (see ref. 8). Treatment of the stress concentration at the edge of the hole requires further analysis, including plasticity, fracture mechanics, and life cycle considerations.

One approach to reducing the stress concentration at the hole is to increase the flange thickness, which reduces the average flange stress and, consequently, the local stress. Figure 15 shows that as flange thickness was increased from 3/4 in. to $1^{1}/_{4}$ in., the peak element circumferential stress decreased from 278 ksi to 227 ksi, or only 18 percent. Similarly, the peak nodal circumferential stress decreased from 391 ksi to 302 ksi (as a basis of comparison, the peak nodal circumferential stress from the refined model of the design with 180 1-in-diameter studs, O-ring side, is 359 ksi for a 3/4-in-thick flange). At the same time, the joint mass penalty increased 18 percent from 1430 lbm to 1752 lbm (or 163 lbm per 1/4 in. of flange thickness). When the increase in joint mass is considered, increasing flange thickness to reduce the peak stress at the edge of the hole appears to be an inefficient way to design a flight weight joint.

If the stress concentration around the hole proves unacceptable, however, a novel method for reducing the peak stress exists. If circumferential slots are cut in the flange tangent to the hole and extended to the gusset (see fig. 8(b)), the flange no longer behaves as a plate with a hole, but as two concentric rings connected by the gussets. This modification largely eliminates the stress concentration. In this model, the bearing plate takes on increased significance, because it must now transfer the nut bearing load to the inner and outer rings and the middle tab. The tab of material between the inner and outer rings has been retained so that the bearing plate does not span too large a distance and aids in restraining the middle of the gusset.

The shaded areas in figure 16 show the locations at the hole edge of the refined mesh model (at a radial cut taken through the stud centerline) with elastic stresses greater than yield (180 ksi) for the design with 180 1-in-diameter studs with a flange/bearing-plate thickness ratio of 0.75 in/0.25 in. Areas on

the unmodified flange both inboard and outboard of the stud where the circumferential elastic stress component is greater than yield are shown in figure 16(a). The peak element elastic stress at the hole edge is 340 ksi. With the slots cut in the flange, however, only a region on the bottom of the outboard ring has stresses greater than yield, and the peak stress at the hole edge is reduced to 223 ksi, as shown in figure 16(b). The bottom of the outer ring still exceeds yield because of flange bending induced by the axial load in the gusset. When the outer flange ring with slots is also cut radially (as depicted in fig. 8(a)), only a small area exceeding yield remains at the outer O-ring groove, and the peak circumferential element stress at the hole edge is further reduced to 178 ksi, as shown in figure 16(c). Cutting the slots and the outer flange results in small increases in gap openings at the O-ring grooves (see R6 in table V) and small increases in gusset axial stress (see fig. 13).

Joint Mass

Any mass added to the SRM, as in joint modifications, reduces the Shuttle payload capability. An indicator of case joint design efficiency is mass penalty, defined here as the mass of the case segment with a joint minus the mass of an equivalent length of shell without a joint. In figure 17, the mass penalty is presented for the bolted joint concept with various stud sizes and alcove modifications. The mass penalties of the original tang-clevis design that flew on mission 51-L and the capture tang redesign, both calculated from dimensions given in reference 8, are also shown. The proposed capture tang has a mass penalty of 932 lbm, which is 180 lbm greater than the penalty of the original joint.

Figure 17 shows the reduction in mass penalty obtained by using a larger number of smaller studs in the bolted joint concept. The data points at 1 in. and $1\frac{1}{16}$ in. are for the refined model described herein and in reference 2, with a flange/bearing-plate thickness ratio of 0.75 in/0.25 in. and an eccentricity of −0.5 in. The intermediate alcove modification to the design with 180 1-in-diameter studs, in addition to lowering the peak stress at the alcove, also removes mass, and consequently reduces the mass penalty of the design by 182 lbm to 1096 lbm. The resulting mass difference between this design and the capture tang redesign is 164 lbm per joint. For the wide-alcove design, the mass penalty is further reduced to 1060 lbm.

The designs with 150 $1\frac{1}{8}$-in-diameter studs (ref. 4) and 144 $1\frac{1}{4}$-in-diameter studs (ref. 3) both have 1-in-thick flanges. The mass penalty for the design with 135 $1\frac{3}{16}$-in-diameter studs (ref. 5) is high (1918 lbm) because the optimization procedure reduced the stress concentration at the edge of the hole solely by increasing flange thickness, resulting in a design with a 1.73-in-thick flange.

Conclusions

The structural design of a bolted joint with a static face seal that can be used to join Space Shuttle solid rocket motor (SRM) case segments is presented. Results from finite-element analyses indicate that the bolted joint meets the design requirement of preventing joint opening at the O-ring locations during SRM pressurization. Results based on a large number of parametric analyses lead to the following conclusions:

1. Negative eccentricity between the shell wall and stud centerlines is an efficient means for preventing joint opening, requiring a mass penalty increase of only 8.0 lbm per 0.1 in. of eccentricity.
2. The smallest joint opening at the O-ring locations and the minimum joint mass penalty are achieved by using the smallest practical (as dictated by gusset axial stress) stud size.
3. Increasing flange thickness above the minimum required to safely carry the joint hoop stress increases the mass penalty without significantly reducing joint opening at the O-ring locations.
4. Localized material tailoring can significantly reduce peak stresses in the gusset and alcove regions of the joint.
5. Because of the substantial mass penalty involved, increasing the flange thickness is an inefficient method of reducing the stress concentration at the hole.
6. Cutting circumferential slots in the flange eliminates the stress concentration at the stud holes, greatly reducing the maximum circumferential flange stress.
7. A final design recommended for further development has the following parameters: 180 1-in-diameter studs, eccentricity of −0.5 in., flange thickness of 0.75 in., bearing-plate thickness of 0.25 in., studs prestressed to 70 percent of ultimate strength, and the intermediate alcove. The resulting design has a mass penalty of 1096 lbm, which is 164 lbm greater than the currently proposed capture tang redesign.

NASA Langley Research Center
Hampton, VA 23665-5225
September 19, 1988

References

1. Presidential Commission on the Space Shuttle Challenger Accident: *Report of the Presidential Commission on the Space Shuttle Challenger Accident, Volumes I–V.* June 6, 1986.

2. Dorsey, John T.; Stein, Peter A.; and Bush, Harold G.: *Structural Design of an In-Line Bolted Joint for the Space Shuttle Rocket Motor Case Segments*. NASA TM-89027, 1987.
3. *LaRC Conceptual Design of Solid Rocket Booster In-Line Bolted Joint*. NASA TM-89046, 1986.
4. Lindell, Michael C.; and Stalnaker, Winifred A.: Structural Analysis of a Bolted Joint Concept for the Space Shuttle's Solid Rocket Motor Casing. AIAA-87-1984, June 1987.
5. Barthelemy, Jean-François M.; Chang, Kwan J.; and Rogers, James L., Jr.: Structural Optimization of an Alternate Design for the Space Shuttle Solid Rocket Booster Field Joint. *A Collection of Technical Papers, Part 1—AIAA/ASME/ASCE/AHS 28th Structures, Structural Dynamics and Materials Conference*, Apr. 1987, pp. 17–26. (Available as AIAA-87-0702.)
6. Dorsey, John T.: *Structural Analysis of the Space Shuttle Solid Rocket Booster/External Tank Attach Ring*. NASA TM-100510, 1988.
7. Whetstone, W. D.: *User Instructions—EISI-EAL Version 312.08*. Engineering Information Systems, Inc., Aug. 1985 (Interim Release).
8. Greene, William H.; Knight, Norman F., Jr.; and Stockwell, Alan E.: *Structural Behavior of the Space Shuttle SRM Tang-Clevis Joint*. NASA TM-89018, 1986.
9. Baumeister, Theodore; Avallone, Eugene A.; and Baumeister, Theodore, III, eds.: *Marks' Standard Handbook for Mechanical Engineers*, Eighth ed. McGraw-Hill Book Co., c.1978.

Table I. Material Properties

	Nut and bearing plate	Stud	Shell wall
Material	Inconel 718	MP 35N	D6AC
Tensile ultimate stress, psi	265 000	273 000	200 000
Tensile yield stress, psi	215 000	263 000	180 000
Allowable stress, psi	189 000	195 000	143 000
Young's modulus, psi	29.7×10^6	35.9×10^6	30.0×10^6

Table II. Gap Magnitudes for Several Flange Thicknesses and Stud Preloads

[170 1 1/16-in. studs, eccentricity of −0.5 in., coarse model]

Flange characteristics	Stud preload, percent	Gap, mils, at location—						
		C1	C2	C3	C4	C5	C6	C7
Solid flange, 1 in. thick	70	0	0.28	0.34	0	0.12	0	4.56
	65	0	.20	.26	0	.11	0	5.03
	60	0	.06	.15	0	.07	.42	5.81
3/4-in-thick flange, 1/4-in. bearing plate	70	0	0	0	0	.18	0	8.89
1-in-thick flange, 1/4-in. bearing plate	70	0	.37	.44	0	.16	0	4.01
1 1/4-in-thick flange, 1/4-in. bearing plate	70	0	.43	.55	0	.10	0	1.79

Table III. Gap Magnitudes for 180-, 170-, and 166-Stud Designs

[1-in-thick flange, eccentricity of −0.5 in., coarse model]

Number and size of studs	Gap, mils, at location—						
	C1	C2	C3	C4	C5	C6	C7
180 1-in. studs	0	0.80	0.16	0	0.03	0	5.03
170 1 1/16-in. studs	0	.28	.34	0	.12	0	4.56
166 1 1/16-in. studs	0	.35	.38	0	.19	0	5.27

Table IV. Gap Magnitudes for 170- and 180-Stud Designs

[3/4-in. flange, 1/4-in. bearing plate, eccentricity of −0.5 in., O-ring side]

Joint design	Gap, mils, at location—							
	R1	R2	R3	R4	R5	R6	R7	R8
180 1-in. studs	0	0.05	0	0	0	0.17	0	8.28
170 1 1/16-in. studs	.08	.17	0	0	0	.24	0	9.18

Table V. Gap Magnitudes for Design With 180 1-in. Studs With Various Flange Modifications

[3/4-in. flange, 1/4-in. bearing plate, eccentricity of −0.5 in.]

Flange characteristics	Gap, mils, at location—							
	R1	R2	R3	R4	R5	R6	R7	R8
O-ring side	0	0.05	0	0	0	0.17	0	8.28
Flat side	0	0	0	0	0	.24	0	8.23
O-ring side (with slots)	.03	0	0	0	0	.15	.88	11.08
Flat side (with slots)	.02	0	0	0	0	.38	.84	11.01
O-ring side (with slots and split flange)	0	0	0	0	0	.04	.05	15.72
Flat side (with slots and split flange)	0	0	0	0	0	.55	.02	15.37
O-ring side (intermediate alcove)	.06	.21	0	.09	0	.28	0	7.74
O-ring side (wide alcove)	.14	.36	0	.24	0	.36	0	7.50

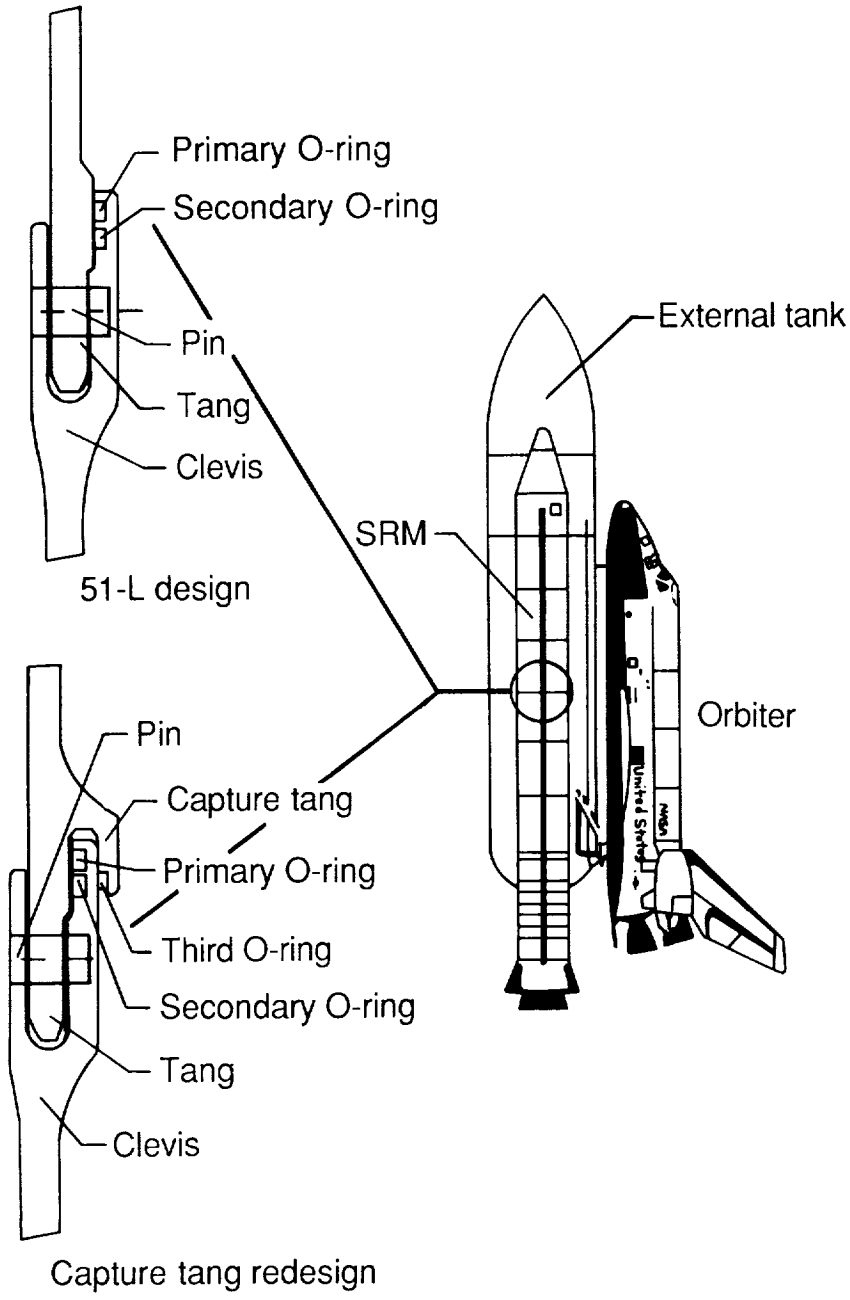

Figure 1. Tang-clevis joints for connecting solid rocket motor case segments.

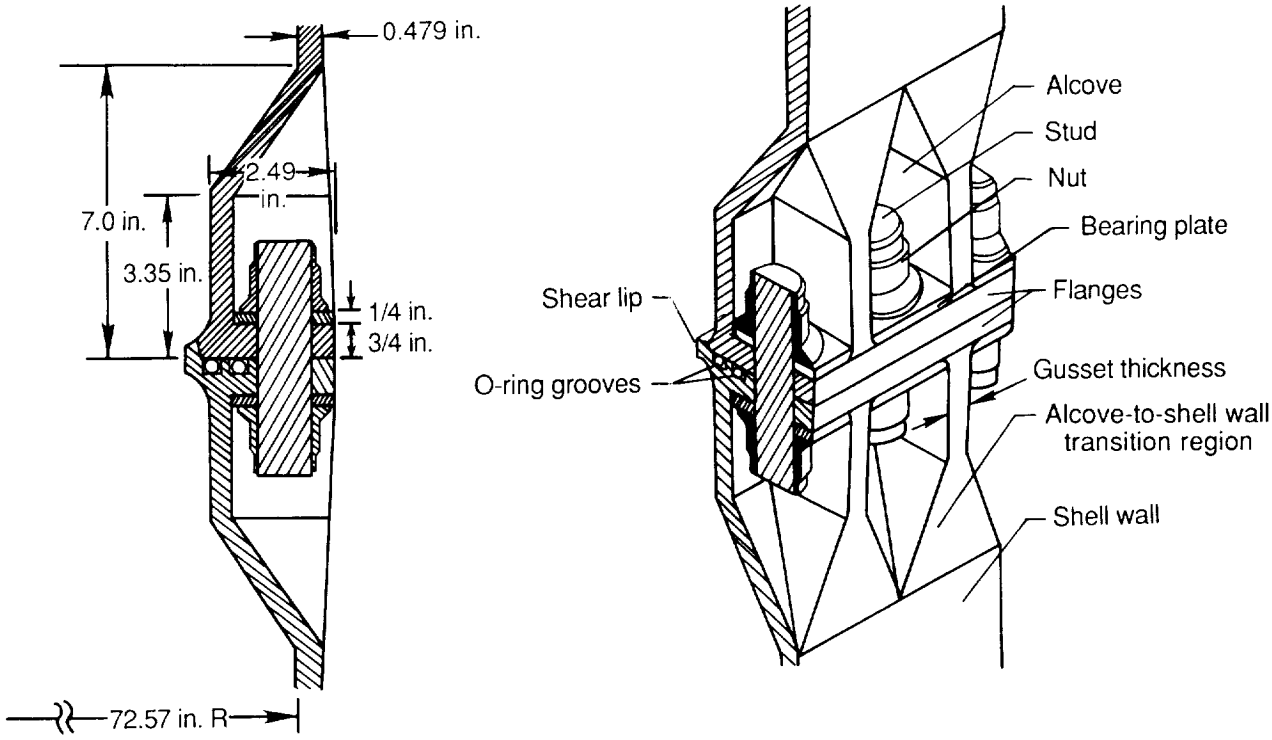

Figure 2. Bolted joint concept.

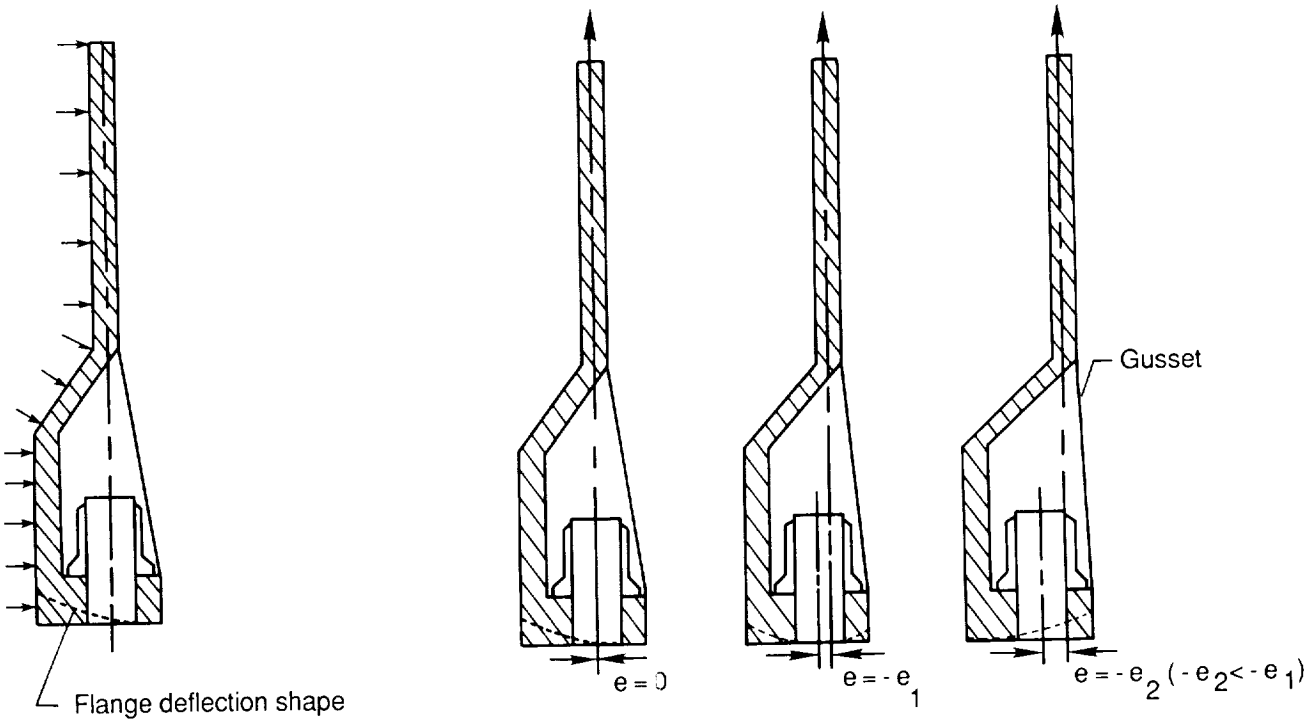

(a) Joint opening due to radial loading.

(b) Joint opening due to axial loading.

Figure 3. Effect of stud centerline eccentricity, e, on joint opening behavior.

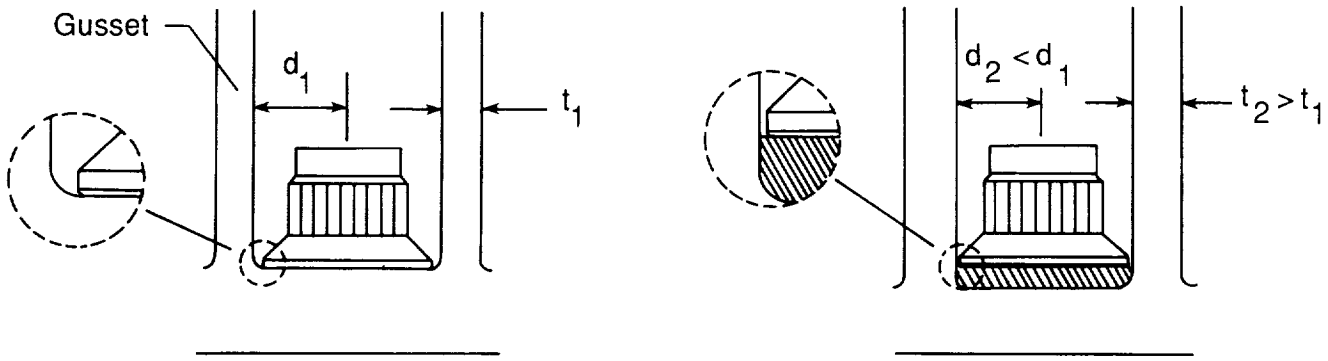

(a) Without bearing plate.

(b) With bearing plate.

Figure 4. Effect of bearing plate on gusset thickness.

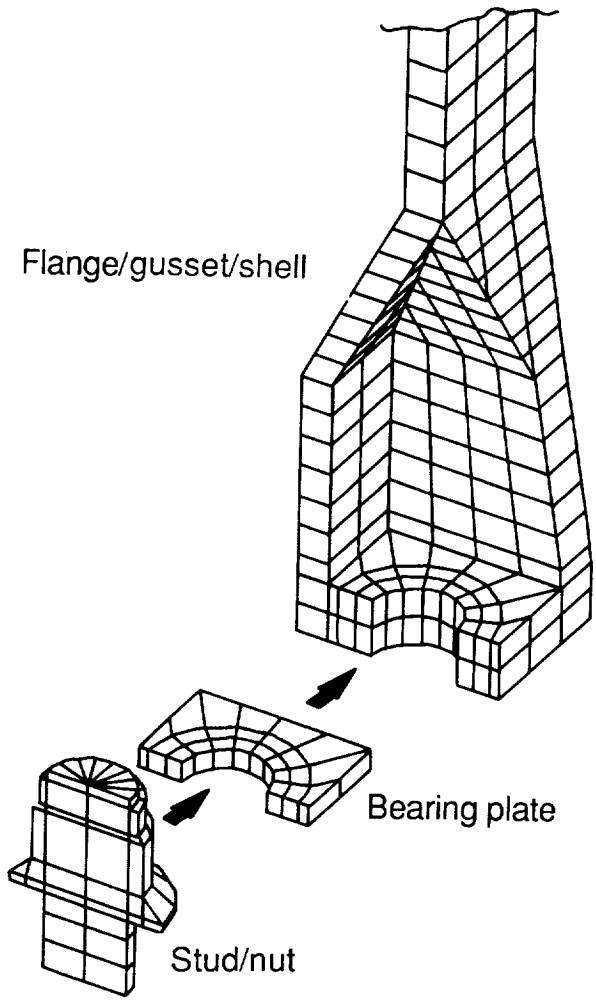

Figure 5. Finite-element subcomponent models (coarse mesh shown).

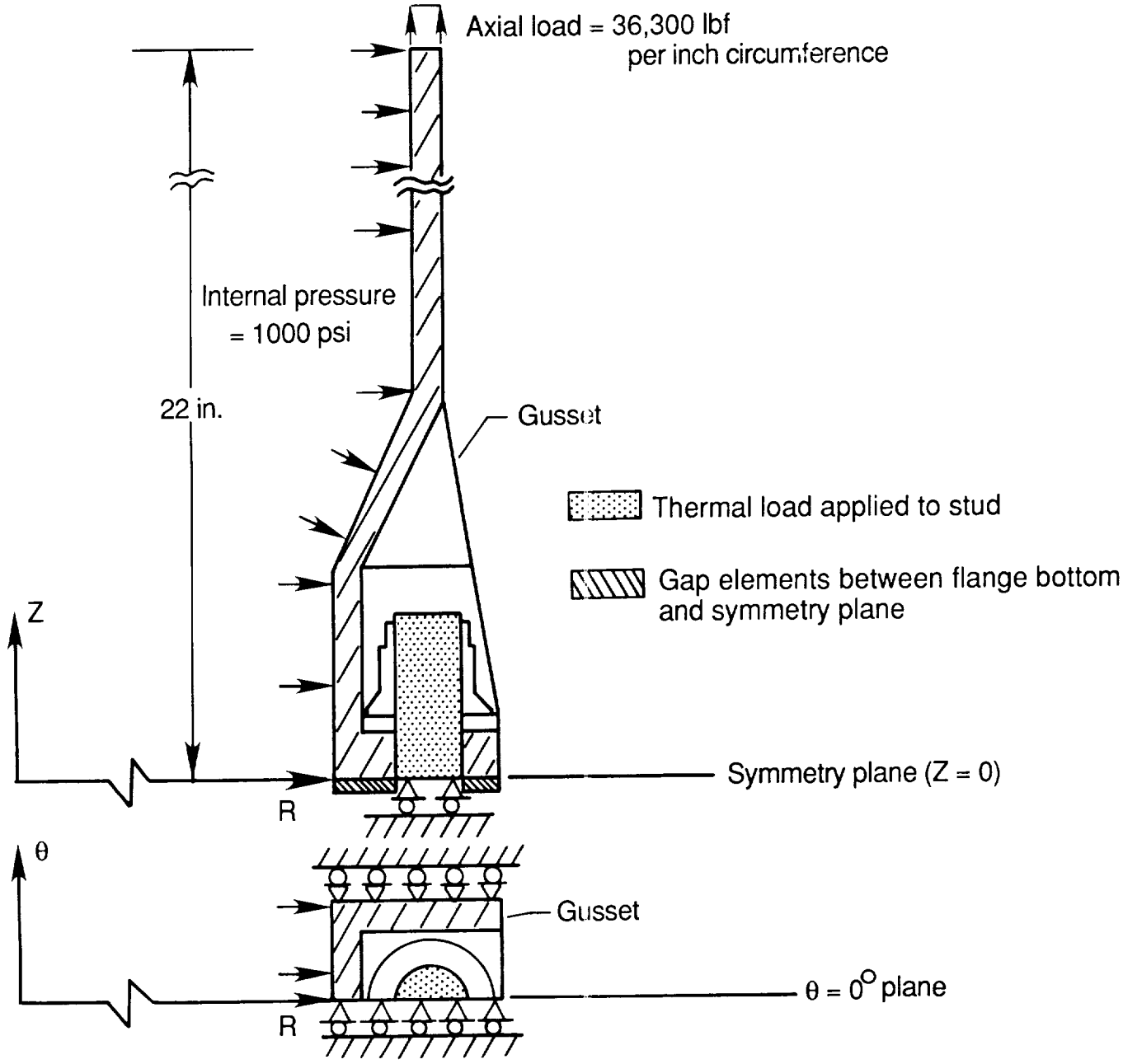

Figure 6. Finite-element model boundary conditions and applied loadings.

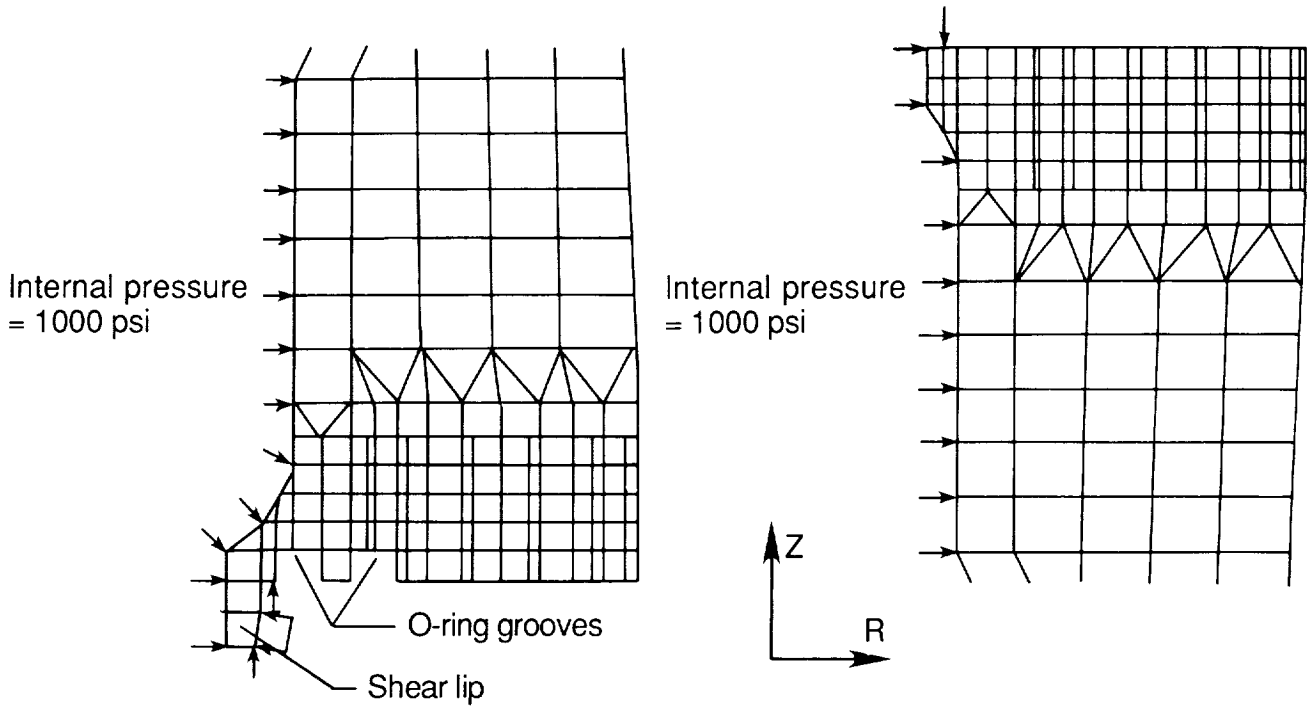

(a) O-ring side. (b) Flat side.

Figure 7. Refined finite-element model.

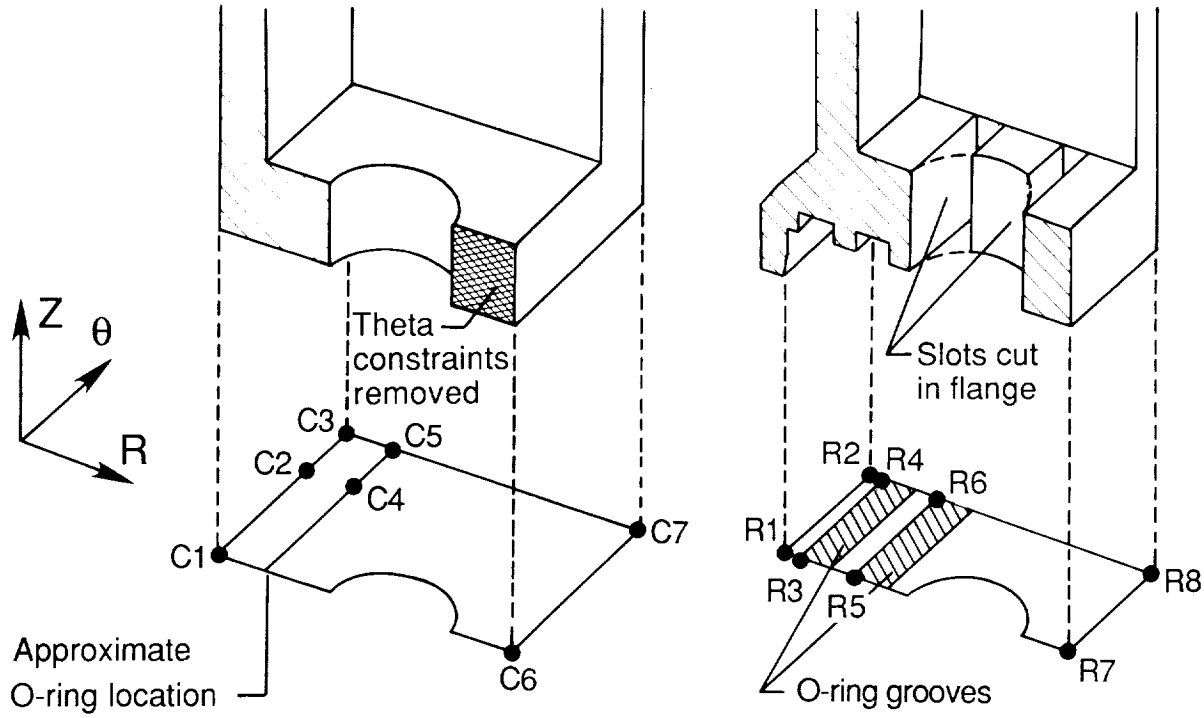

(a) Coarse model. (b) Refined model, O-ring side.

Figure 8. Gap locations on flange bottom.

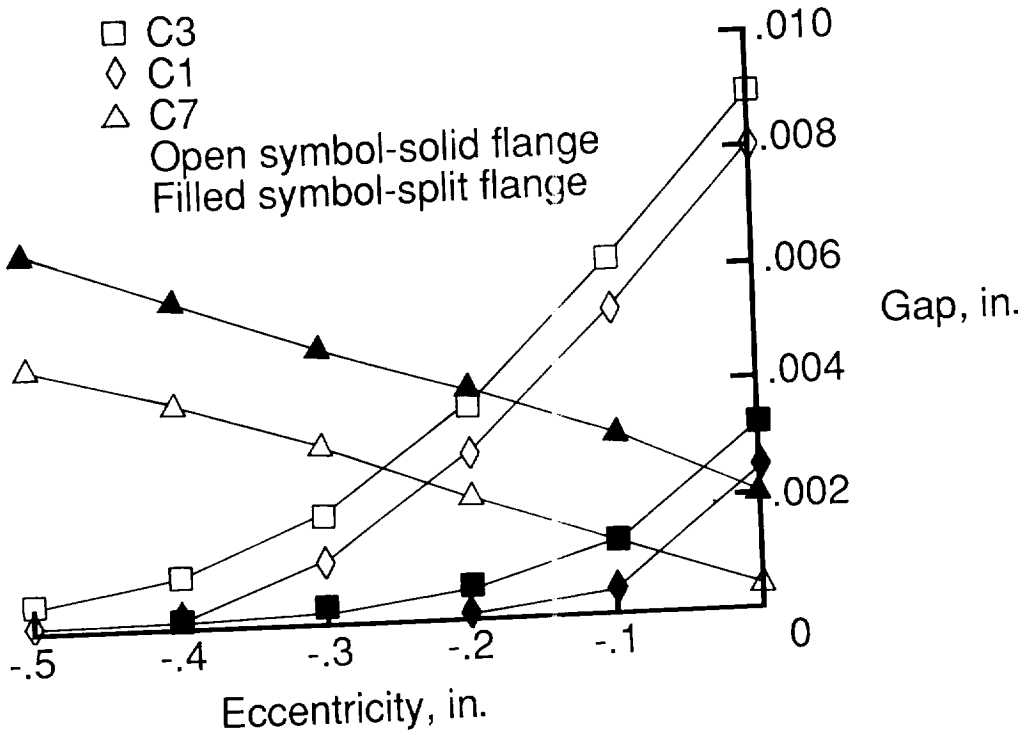

Figure 9. Gap magnitude on flange bottom as a function of stud eccentricity.

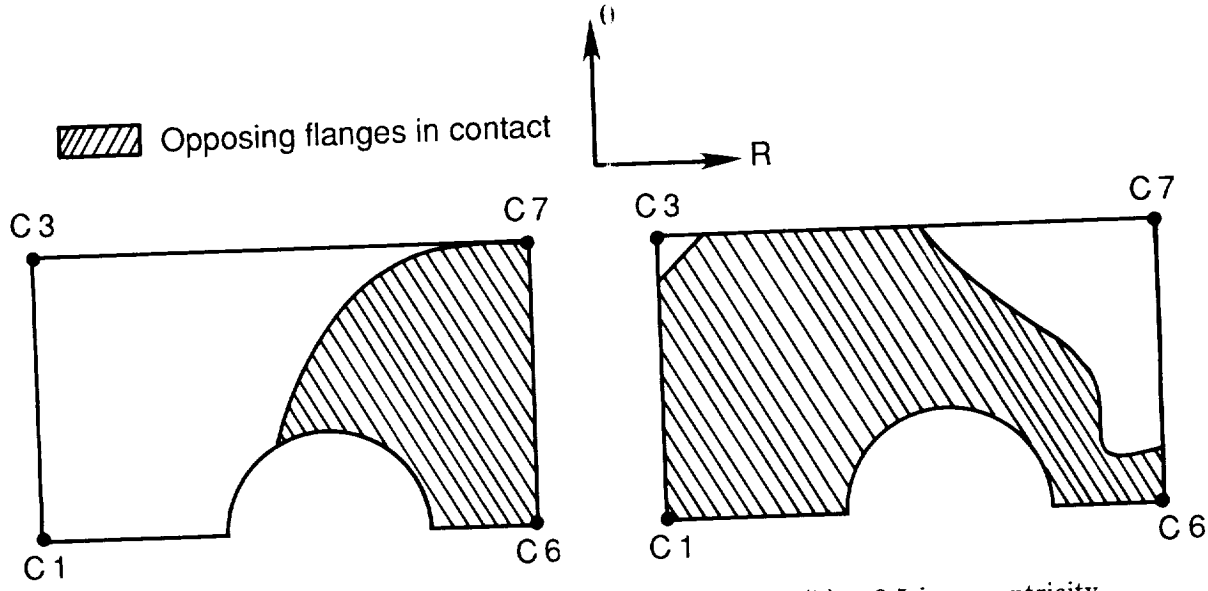

(a) No eccentricity.

(b) −0.5 in. eccentricity.

Figure 10. Approximate contact region on flange bottom for two values of stud eccentricity (coarse model). (Internal pressure = 1000 psi.)

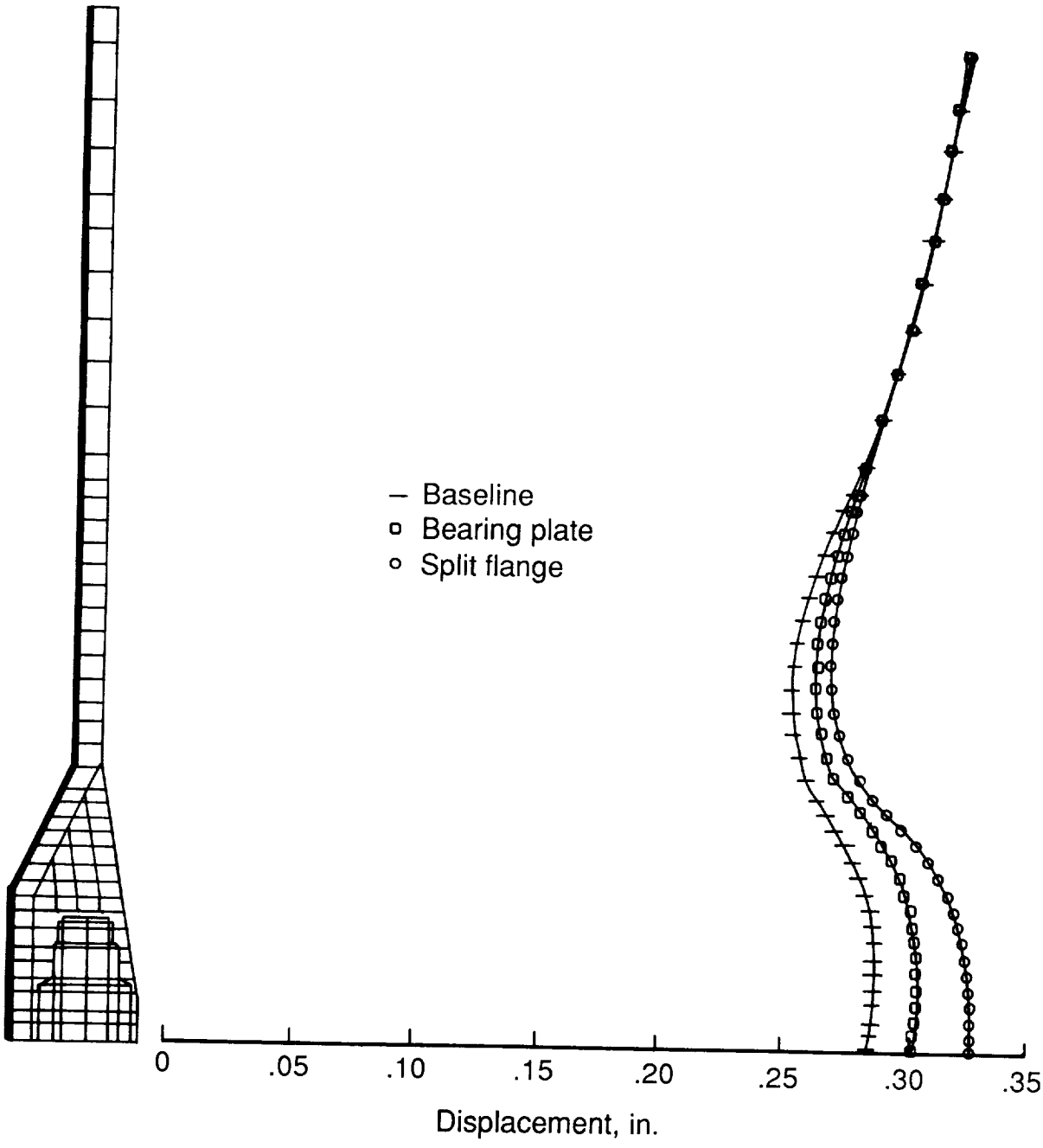

Figure 11. Radial displacement increases caused by flange hoop-stiffness reductions.

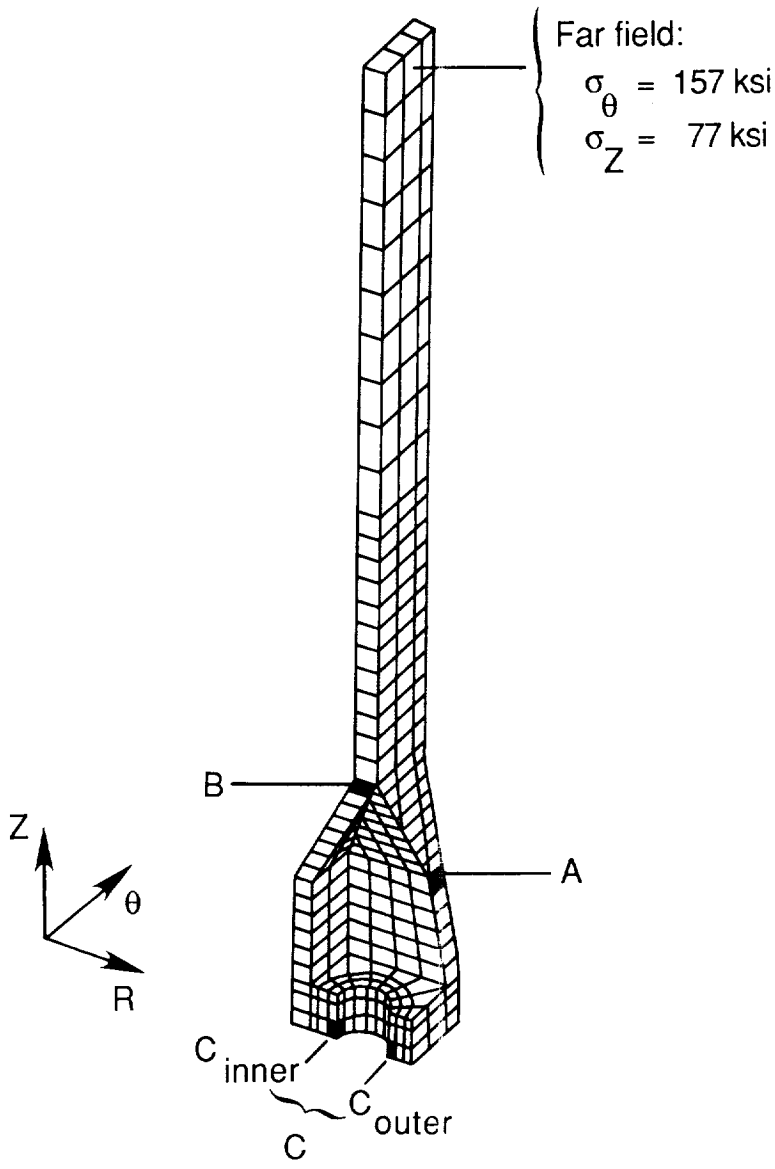

Figure 12. Stress concentration locations.

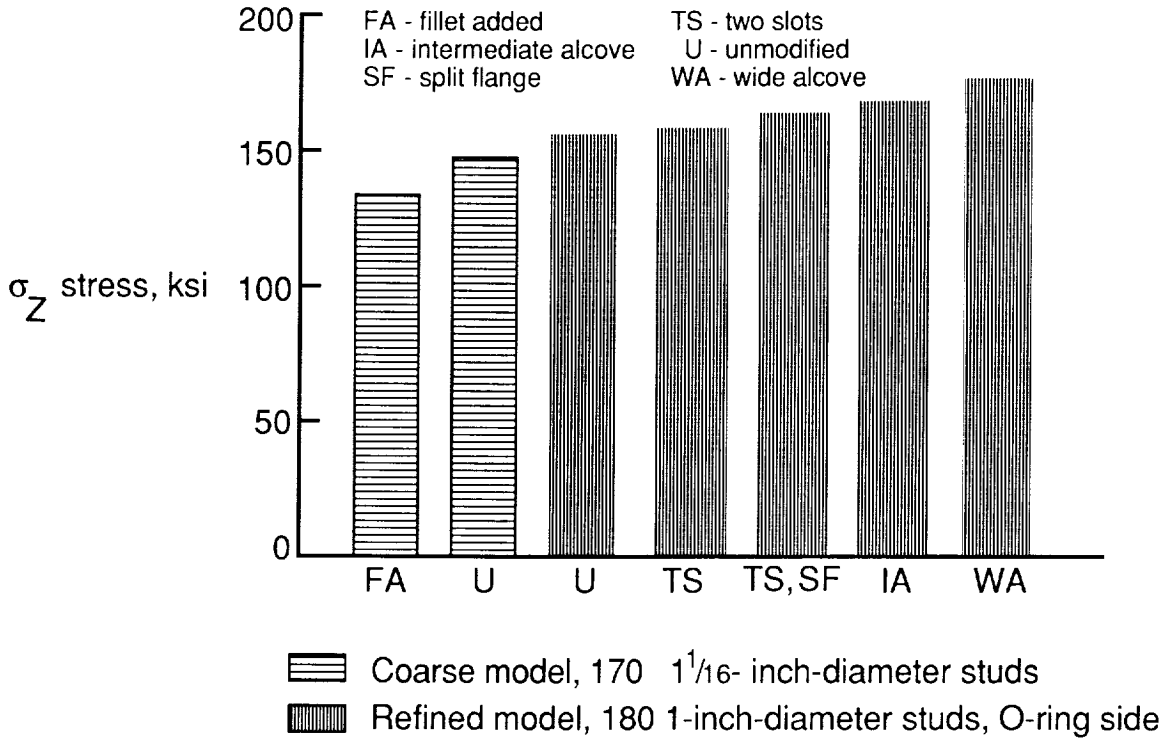

Figure 13. Variations in gusset axial stress with model modifications. Both models have 3/4-in-thick flanges, 1/4-in-thick bearing plates, and eccentricity of −0.5 in.

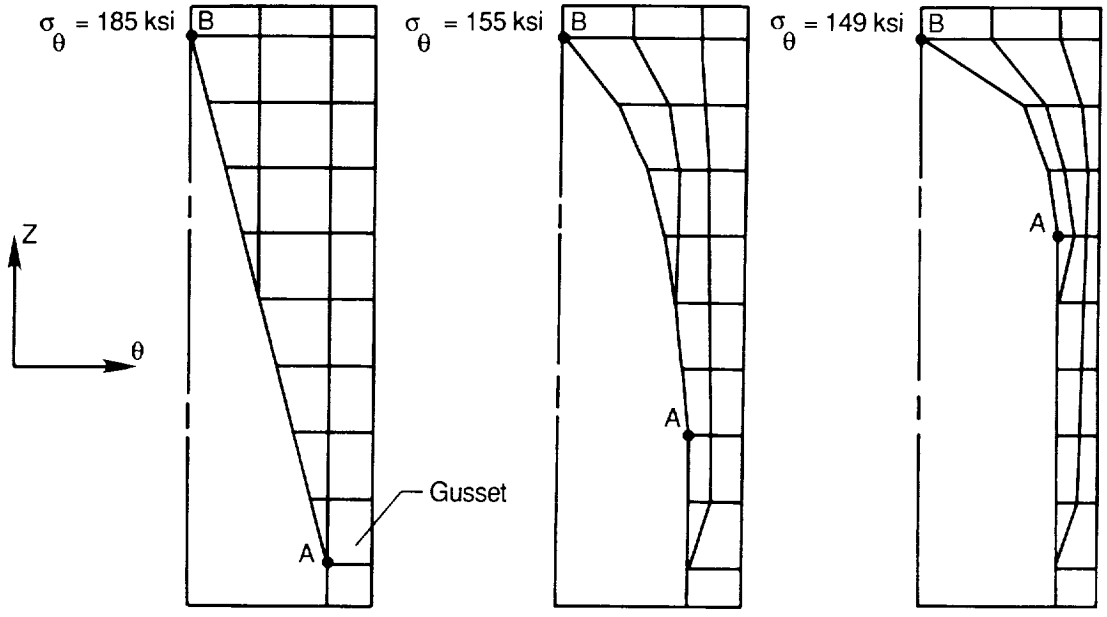

(a) Original alcove. (b) Intermediate alcove. (c) Wide alcove.

Figure 14. Alcove tailoring (material removal) schemes (radial view). A denotes peak stress location at gusset/wedge intersection. B denotes peak stress location at top of alcove.

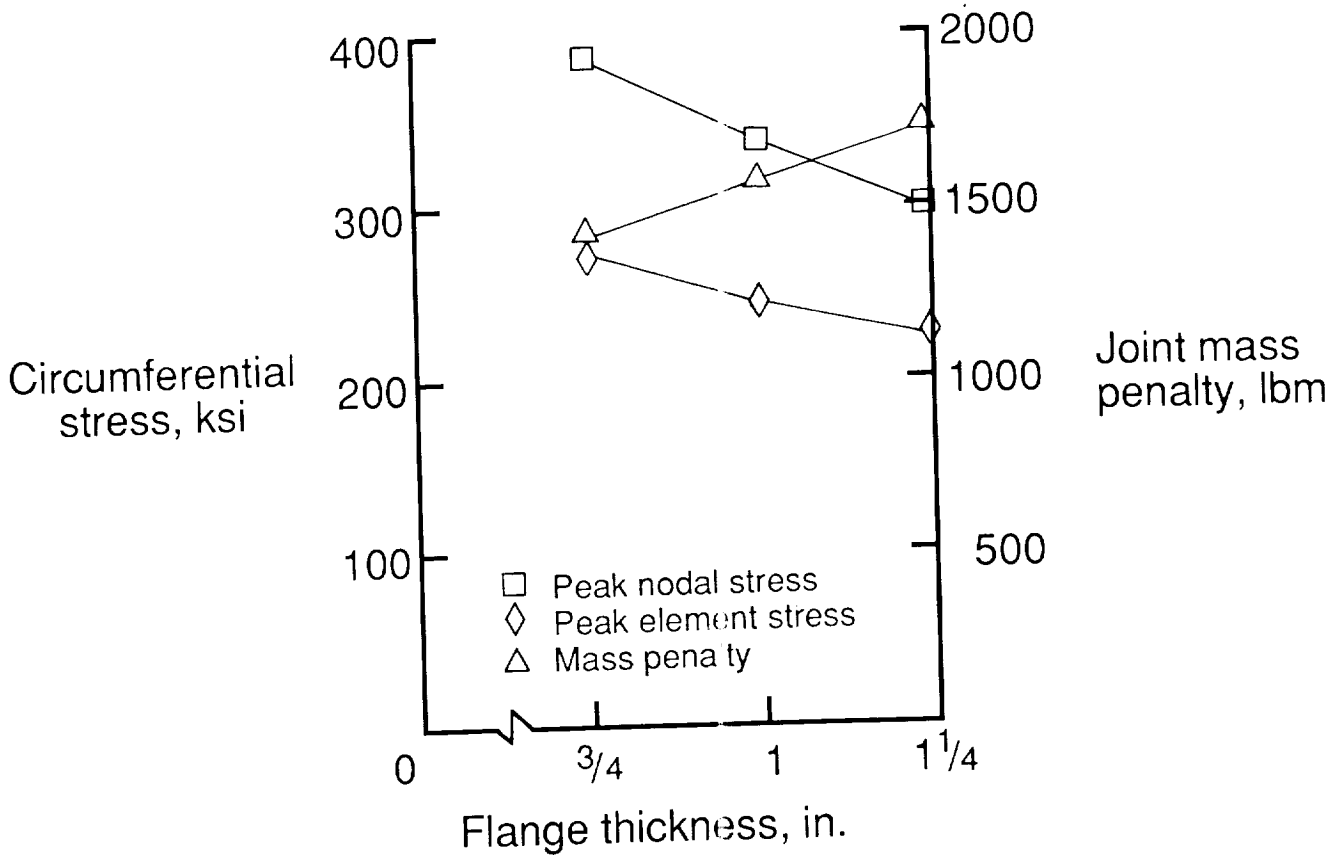

Figure 15. Maximum tensile stress at hole edge as a function of flange thickness.

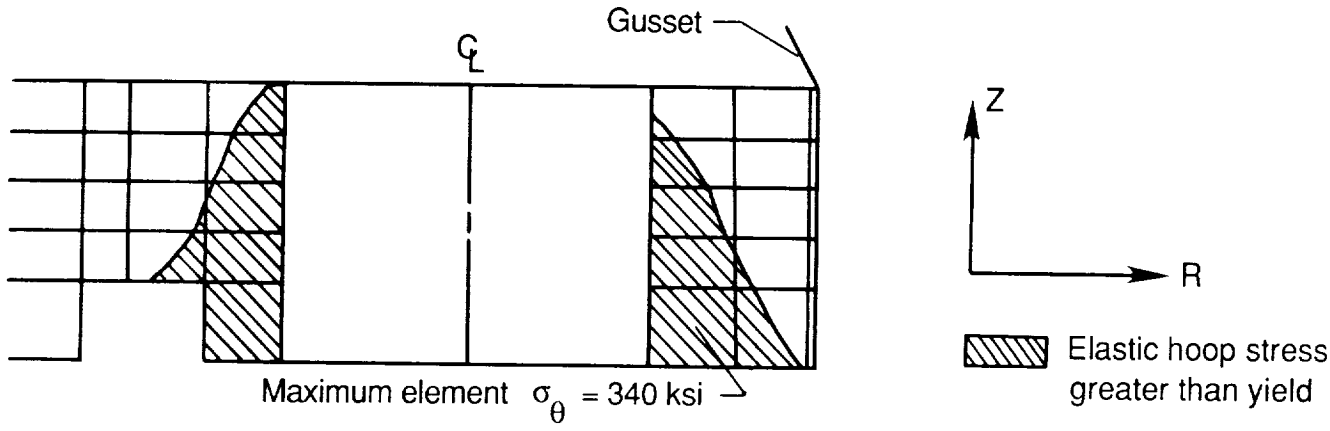

(a) Unmodified flange.

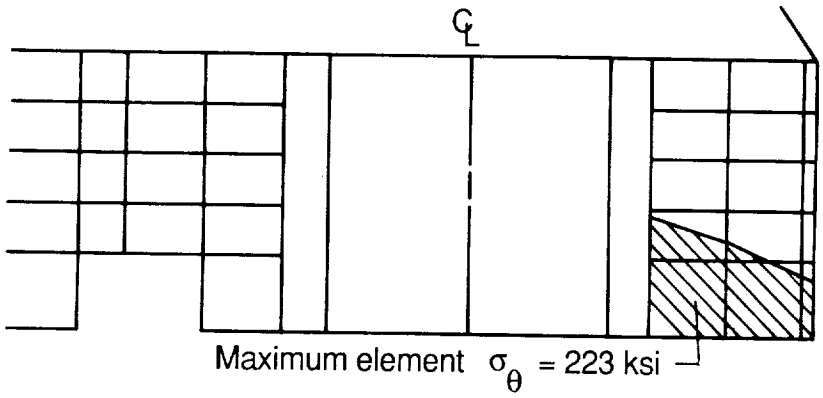

(b) Two slots in flange.

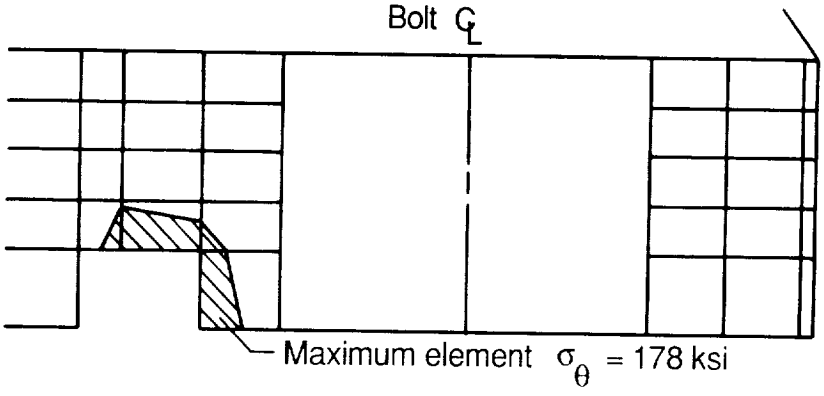

(c) Two slots, split flange.

Figure 16. Regions near hole edge with elastic hoop stress above yield. (Circumferential view of radial cut through $\theta = 0$ plane.)

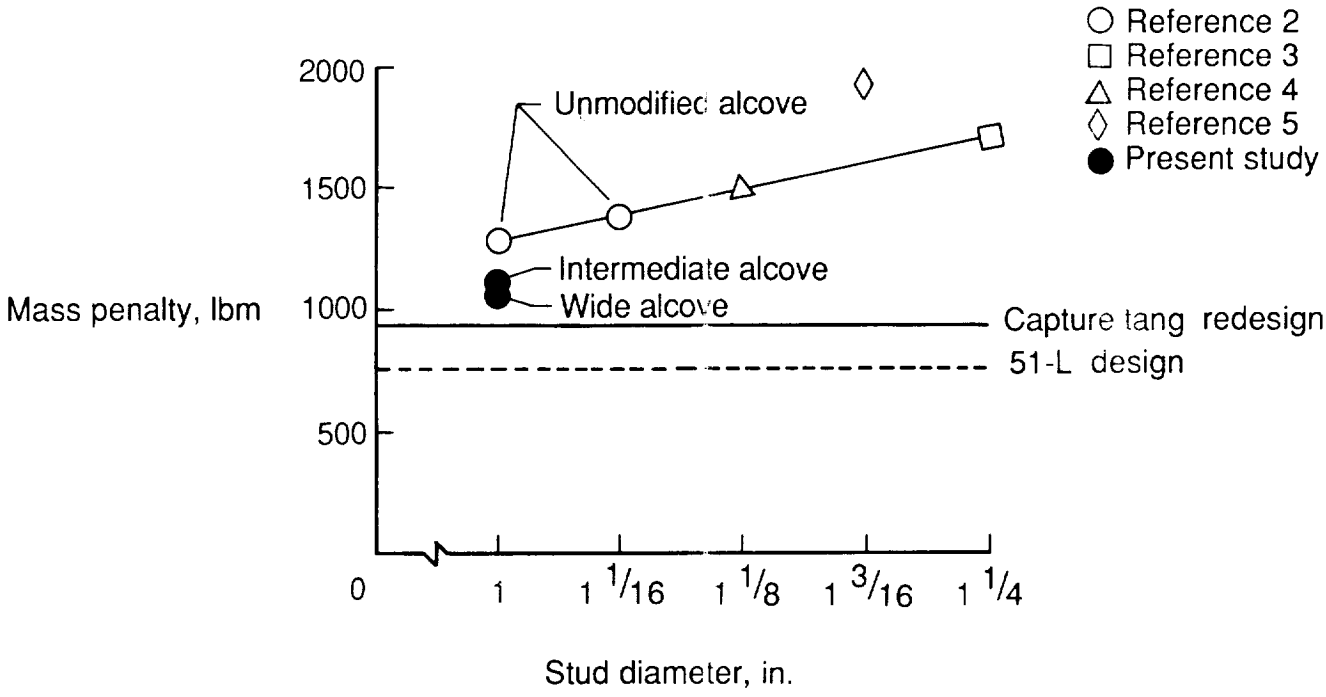

Figure 17. Mass penalty per joint for various case segment joint designs.

NASA
National Aeronautics and Space Administration

Report Documentation Page

1. Report No.	2. Government Accession No.	3. Recipient's Catalog No.
NASA TP-2851		

4. Title and Subtitle	5. Report Date
Lightweight Structural Design of a Bolted Case Joint for the Space Shuttle Solid Rocket Motor	November 1988
	6. Performing Organization Code
7. Author(s)	8. Performing Organization Report No.
John T. Dorsey, Peter A. Stein, and Harold G. Bush	L-16496
9. Performing Organization Name and Address	10. Work Unit No.
NASA Langley Research Center Hampton, VA 23665-5225	506-43-41-02
	11. Contract or Grant No.
12. Sponsoring Agency Name and Address	13. Type of Report and Period Covered
National Aeronautics and Space Administration Washington, DC 20546-0001	Technical Paper
	14. Sponsoring Agency Code

15. Supplementary Notes

John T. Dorsey and Harold G. Bush: Langley Research Center, Hampton, Virginia.
Peter A. Stein: U.S. Coast Guard Station, Yorktown, Virginia.

16. Abstract

This paper presents the structural design of a bolted joint with a static face seal that can be used to join Space Shuttle solid rocket motor (SRM) case segments. Results from numerous finite-element parametric studies indicate that the bolted joint meets the design requirement of preventing joint opening at the O-ring locations during SRM pressurization. A final design recommended for further development has the following parameters: 180 1-in-diameter studs, stud centerline offset of 0.5 in. radially inward from the shell wall centerline, flange thickness of 0.75 in., bearing-plate thickness of 0.25 in., studs prestressed to 70 percent of ultimate load, and the intermediate alcove. The design has a mass penalty of 1096 lbm, which is 164 lbm greater than the currently proposed capture tang redesign.

17. Key Words (Suggested by Authors(s))	18. Distribution Statement
Space Shuttle solid rocket motor (SRM) Bolted joint Rocket motor case segment joints	Unclassified—Unlimited Subject Category 18

19. Security Classif.(of this report)	20. Security Classif.(of this page)	21. No. of Pages	22. Price
Unclassified	Unclassified	22	A02

For sale by the National Technical Information Service, Springfield, Virginia 22161-2171